

# Bimetallic Bi/Zn decorated hydrothermally synthesized TiO<sub>2</sub> for efficient photocatalytic degradation of nitrobenzene

Preeti<sup>a</sup>, Saurav Mishra<sup>a</sup>, Nandana Chakinala<sup>b</sup>, Anand G. Chakinala<sup>b,\*</sup>, Praveen K. Surolia<sup>a,\*</sup>

<sup>a</sup> Solar Energy Conversion and Nanomaterials Laboratory, Department of Chemistry, Manipal University Jaipur, Jaipur, 303007, Rajasthan, India

<sup>b</sup> Chemical Reaction Engineering Laboratory, Department of Chemical Engineering, Manipal University Jaipur, Jaipur, 303007, Rajasthan, India

## ARTICLE INFO

### Keywords:

Photocatalytic degradation  
M-doped TiO<sub>2</sub> (M-Bi, Zn)  
Hydrothermal synthesis  
Surface plasma resonance

## ABSTRACT

Semiconductor photocatalyst TiO<sub>2</sub> was synthesized by hydrothermal method, followed by Bi/Zn mono and bimetallic nanoparticles decorated through wet impregnation. Metal doping resulted a shift in spectral response to visible light, with highest shift of 0.08 eV in BZHT4 (0.25:0.75 w/w). Photocatalytic performances of synthesized catalysts were compared for the degradation of 50 ppm nitrobenzene (NB) under UV and solar light irradiations. Enhanced photocatalytic activity was observed with the metal doping due to the synergistic effects between the metals and TiO<sub>2</sub>. Highest degradation of 90% with a rate constant of  $8.8 \times 10^{-3} \text{ min}^{-1}$  was observed with BZHT4 in UV light.

## 1. Introduction

The wastewater released during various industrial manufacturing operations can cause serious water problems and may pose a serious threat to the ecosystem and human health [1]. Recently, photocatalytic degradation process with semiconductor TiO<sub>2</sub> utilizing solar and ultraviolet (UV) light has become an important aspect for the decomposition of organic pollutants because of its low cost, chemical stability, non-toxicity, electronic and optical properties [2–5]. Important factors which affect the photocatalytic activity of TiO<sub>2</sub> are crystallinity, specific surface area, shape and size [6]. The major disadvantage of TiO<sub>2</sub> is its wide band gap (3.0–3.2 eV) which indicate that only a small percentage of solar spectra is absorbed in the UV region and low quantum efficiency owing to the fast recombination. Several techniques have been applied to lower the band gap, some of which include synthesis of particles with different nanostructure, doping of metals and non-metals, and the preparation of nanocomposites [6,7]. Doping can decrease the band gap between valance band and conduction band through the addition of impurities in the pure semiconductor [8,9]. Transition metal doped TiO<sub>2</sub> has shown remarkable effects on the photocatalytic degradation [10–12].

Bi-doping introduce a narrow intermediate energy band gap and act as an active centre on the photocatalytic surface for degradation process [13,14]. Bi is a low-cost base metal that is shown to exhibit direct plasmonic photocatalytic ability having the potential to replace the

noble metals. Doping of Bi is known for band gap reduction resulting in the up-shift valence band due to hybridization of Bi (6s) orbital with O (2p) orbital [15]. Hence, it is anticipated that the addition of Bi will be successful in extending the spectral response of TiO<sub>2</sub> to the visible light region. Further, doping of Zn<sup>2+</sup> on TiO<sub>2</sub> was reported to ease the electron injection and enhance the charge collection owing to excess holes of Zn<sup>2+</sup> as compared to Ti<sup>4+</sup> that forms an acceptor level near to the valence band of TiO<sub>2</sub> [16]. Co-doping of Bi and Zn on TiO<sub>2</sub> have been reported to inhibit the recombination of electron-hole pairs in photocatalytic degradation of organic contaminants [13,17]. In addition, the photogenerated holes (*h*<sup>+</sup>) were accounted as the main active species for the degradation of organic pollutants, with contributions of O<sub>2</sub><sup>•-</sup> and HO<sup>•</sup> being moderate and small respectively. Moreover, the co-doped catalyst was also reported to exhibit good stability in terms of achieving the same performance for five cycles [17]. Therefore, the outcome of these reports triggered to apply Bi–Zn combined doping over hydrothermally synthesized TiO<sub>2</sub> in this work.

In this study, TiO<sub>2</sub> photocatalyst was synthesized using hydrothermal method and subsequent doping with Bi and Zn (mono- and bimetallic) was carried using wet impregnation method. Synthesized photocatalysts were characterized and tested for the degradation of NB as a model pollutant. Both, Bi and Zn doping were reported to enhance the performance of TiO<sub>2</sub> [17,18,19] and as per our best knowledge, the bimetallic doping of Bi and Zn in combination to hydrothermally synthesized TiO<sub>2</sub> has not been reported so far for the purpose of

\* Corresponding authors.

E-mail addresses: [anandgupta.chakinala@jaipur.manipal.edu](mailto:anandgupta.chakinala@jaipur.manipal.edu) (A.G. Chakinala), [praveenkumar.surolia@jaipur.manipal.edu](mailto:praveenkumar.surolia@jaipur.manipal.edu) (P.K. Surolia).

<https://doi.org/10.1016/j.catcom.2022.106538>

Received 4 September 2022; Received in revised form 14 October 2022; Accepted 18 October 2022

Available online 19 October 2022

1566-7367/© 2022 The Authors. Published by Elsevier B.V. This is an open access article under the CC BY-NC-ND license (<http://creativecommons.org/licenses/by-nc-nd/4.0/>).

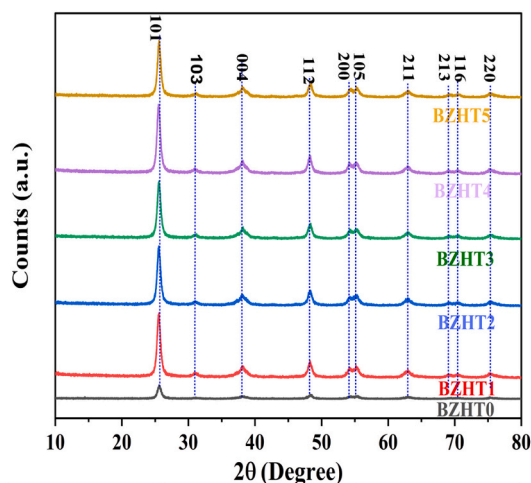


Fig. 1. XRD pattern of the bare and metal doped TiO<sub>2</sub> catalysts.

photocatalytic degradation of organic pollutants in water. The performance of the synthesized photocatalysts is discussed in terms of its charge separation properties of the doped materials.

## 2. Experimental section

### 2.1. Catalyst synthesis

The detailed catalytic preparation procedure is presented in supporting information and schematically illustrated in Fig. S1. The catalyst TiO<sub>2</sub> was prepared via hydrothermal synthesis method. Further, catalysts were impregnated with different % loading of Bi:Zn (*w/w*) on TiO<sub>2</sub> were (1.0:0.0); (0.75:0.25); (0.50:0.50); (0.25:0.75); (0.0:1.0) and named as BZHT1, BZHT2, BZHT3, BZHT4 and BZHT5. Hydrothermally synthesized TiO<sub>2</sub> catalyst without metal doping was denoted as BZHT0.

### 2.2. Catalyst characterization

The characterization of the hydrothermal synthesized and doped TiO<sub>2</sub> was conducted using different characterization techniques such as XRD, DRS, FT-IR, TGA, SEM, PL and details are provided in the supporting information.

### 2.3. Experimental setup and photocatalytic activity study

The photocatalytic reactions were performed both under UV light in a 500 mL capacity reactor set-up using of 250 W mercury vapor lamp (Fig. S2) and under natural solar irradiation (Fig. S3). All tests reported in this study were carried out with 50 ppm of NB solution. Details of the experimental setup and reaction conditions are given in the supporting information.

## 3. Result and discussion

### 3.1. Characterization

The XRD patterns of bare and all doped TiO<sub>2</sub> showed major peak recorded at  $2\theta = 25.6$  (Fig. 1). According to XRD patterns, the predominant structure is anatase with no other TiO<sub>2</sub> phase or impurity phase caused by dopant which signifies that the dopants have been effectively doped into the TiO<sub>2</sub> lattice [13]. It could be due to the lower loading values of Bi and Zn metals (less than 1% *w/w*) [6]. The major diffraction peaks observed in XRD patterns were at  $2\theta = 25.6, 31.06, 38.09, 48.34, 54.38, 55.38, 63, 69.6, 70.48, 75.4$  indexed to (101), (103), (004), (112), (200), (105), (211), (213), and (116). The crystallite sizes were

Table 1

Textural and electronic properties of bare and metal (Bi, Zn) doped TiO<sub>2</sub> Catalysts.

Catalyst	Average crystallite size (nm)	Crystallinity index (%)	Band gap $E_g$ (eV)
BZHT0	26.51	45.63	3.18
BZHT1	28.16	50.65	3.15
BZHT2	27.58	48.41	3.12
BZHT3	28.11	51.49	3.12
BZHT4	27.84	51.86	3.10
BZHT5	29.09	66.10	3.15

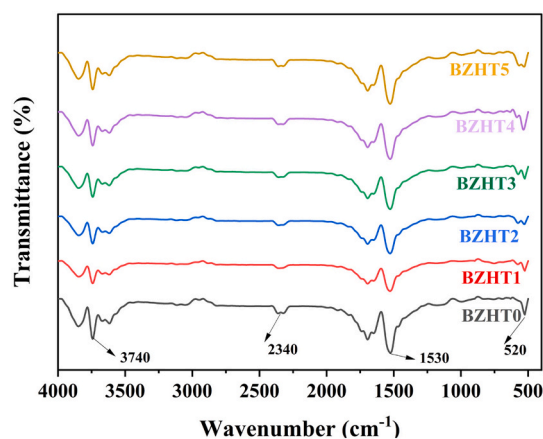


Fig. 2. FTIR spectra of bare and metal doped TiO<sub>2</sub> catalysts.

calculated using Scherrer's formula, with the characteristic peak of  $2\theta = 25.6$ , with a shape factor (*K*) of 0.9 (Eq. (1)) and were found between 26.51 and 29.09 nm (Table 1). Crystallite sizes were found to be marginally increased after the metal loading, which shows that loading of metals might promote the growth of TiO<sub>2</sub> nanoparticles [20]. The increase in crystallite size could also be due to nanoparticles insertion in surface-layer of TiO<sub>2</sub> support [21]. However, this growth was not that considerable and only a slight difference was observed.

$$\text{Crystallite size} = K\lambda / (W\cos\theta) \quad (1)$$

Where  $W = W_b - W_s$ ,  $W_b$  is the broadened profile width of experimental sample.  $W_s$  is the standard profile width of reference silicon sample, and  $\lambda$  is the wavelength of X-ray radiation [22,23]. The crystallinity index (CI) was calculated using Eq. (2).

$$CI = \frac{\text{Area of crystalline peaks}}{\text{Area of crystalline peaks} + \text{Area of amorphous peaks}} \times 100 \quad (2)$$

The CI value for BZHT0, BZHT1, BZHT2, BZHT3, BZHT4, and BZHT5 were estimated to be 45.63, 50.65, 48.41, 51.49, 51.86 respectively. The marginal increase in the CI values was noticed in the XRD pattern with increased intensity of the peaks in all the metal doped samples. This could be due to the metal loading and extra sintering after the metal loading [24].

FTIR spectra of bare TiO<sub>2</sub> and Bi/Zn impregnated TiO<sub>2</sub> catalysts shown in Fig. 2 depicts (-OH) stretching bands in the range of 3740–3300  $\text{cm}^{-1}$  for all the catalysts. The peak observed at 1500–1750  $\text{cm}^{-1}$  is due to the bending vibrations of H-O-H. The vibration of Ti-O-Ti is represented by the appearance of a band at 450–550  $\text{cm}^{-1}$  range [25,26].

The diffuse reflectance spectra (DRS) of bare TiO<sub>2</sub> and Bi/Zn doped TiO<sub>2</sub> is shown in the Fig. S4 (a) and (b). The band gap energy ( $E_g$ ) of the photocatalysts was calculated using Kubelka-Munk equation (Eq. (3)) as given below [27].

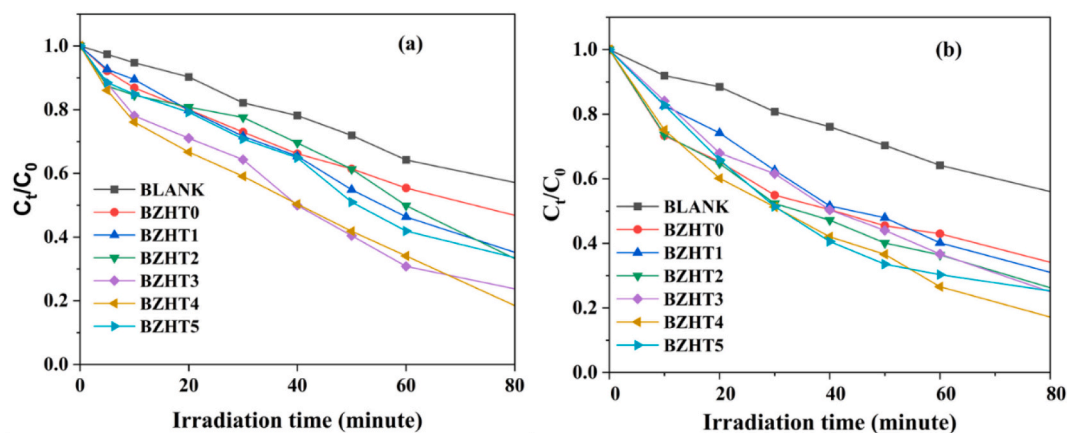


Fig. 3. Concentration profile of nitrobenzene degradation as a function of irradiation time (a) under UV irradiation and (b) solar irradiation.

$$F(R) = \frac{(1 - R^2)}{2R} \quad (3)$$

Where, R represents the measured absolute reflectance of the photocatalyst.

It was observed that after doping with dopants Bi<sup>3+</sup> and Zn<sup>2+</sup>, the photocatalysts intensify the optical absorption to visible light region. The plot of {(R)\*hν} versus photon energy (hν) was used for the calculation of band gap. The intercept of tangent to the plot can provide an approximation of band gap energy of semiconductor catalysts.

Surface morphology of the synthesized catalysts were found to be in spherical agglomerates with typical size less than 100 nm facilitating a better uniform distribution (Fig. S5). A marginal difference in the particle sizes were noticed after doping the metals that is not very significant owing to low metal doping. The existence of metals after the loading was affirmed by EDX analysis. However, EDX analysis could provide the results for the metal particles which were existing only on the TiO<sub>2</sub> surface.

The fate of photoinduced charge carriers can be explored through PL analysis as it is related to the rate of recombination of e<sup>-</sup> and h<sup>+</sup> [28]. The PL spectra of doped and bare TiO<sub>2</sub> are shown in the Fig. S6. In this analysis, all samples were evaluated in the 350–550 nm region. From the spectra it can be understood that the rate of recombination of e<sup>-</sup>/h<sup>+</sup> is directly proportional to the photoluminescence intensity. One dominant peak at 456 nm and another at 419 nm were observed for all doped and bare TiO<sub>2</sub>. It is seen that the peak intensity is higher in all metal doped catalysts over the wide range of spectrum, showing the minimum recombination which may be associated with their band gap values.

Thermal weight loss profiles using thermogravimetric analysis (TGA) (Fig. S7) showed less than 5% weight loss below 150 °C which is mainly due to the removal of moisture content present in the catalyst [29]. No further weight loss was observed which indicates the thermal stability of all the catalysts.

### 3.2. Photocatalytic activity and kinetics of nitrobenzene degradation

The photocatalytic performance of the synthesized catalysts was evaluated for the degradation of NB both in a photocatalytic reactor and under visible solar light irradiation. The degradation profiles of NB under UV and visible solar light irradiation is shown in Fig. 3.

The kinetics of NB degradation was carried out as per Langmuir-Hinshelwood mechanism and the data were fitted to pseudo-first order kinetic model as per Eq. (4).

$$r = \frac{kKC_t}{1 + KC_t} \approx kKC_t = k_{app}C_t \quad (4)$$

Where k is the reaction rate constant, K is the reactant adsorption constant, and C<sub>t</sub> is concentration of NB at any time ‘t’. First order

**Table 2**  
Kinetics data of nitrobenzene degradation in the presence of TiO<sub>2</sub> and M/TiO<sub>2</sub> photocatalysts (M = Bi, Zn) in UV light.

Catalyst	%Degradation (After 90 min)	Initial rate × 10 <sup>-6</sup> (mol min <sup>-1</sup> )	Rate constant (K <sub>app</sub> ) × 10 <sup>-3</sup> (min <sup>-1</sup> )	R <sup>2</sup>
BLANK	30	2.02	2.2	0.96
BZHT0	57	4.03	4.3	0.99
BZHT1	70	3.80	5.4	0.97
BZHT2	75	3.90	5.5	0.95
BZHT3	78	4.86	7.4	0.99
BZHT4	90	6.89	8.8	0.98
BZHT5	70	4.30	5.7	0.98

**Table 3**  
Kinetics data of nitrobenzene degradation in the presence of TiO<sub>2</sub> and M/TiO<sub>2</sub> photocatalysts (M = Bi, Zn) in sunlight.

Catalyst	%Degradation (After 90 min)	Initial rate × 10 <sup>-6</sup> (mol min <sup>-1</sup> )	Rate constant (K <sub>app</sub> ) × 10 <sup>-3</sup> (min <sup>-1</sup> )	R <sup>2</sup>
BLANK	41	2.07	2.5	0.99
BZHT0	70	5.56	6.5	0.97
BZHT1	74	4.50	6.3	0.99
BZHT2	78	6.22	7.8	0.98
BZHT3	80	5.52	7.6	0.99
BZHT4	84	6.99	8.5	0.98
BZHT5	75	6.24	7.8	0.95

kinetics of NB degradation both in UV and natural sunlight is shown in Fig. S8. The calculated rate constants had R<sup>2</sup> values close to linearity are specified in Tables 2 and 3. A clear sharp decrease in the concentration can be seen for first 60 min in all the reaction performed (Fig. 3). This shows highest degradation was completed within first hour only.

It can be clearly seen from Tables 2 and 3 that the metal doping has increased the performance of the TiO<sub>2</sub> photocatalyst which could be attributed to better charge separation compared to bare TiO<sub>2</sub>. Further, among all the prepared catalysts, the final percentage degradation of NB was found to be highest for BZHT4, 84% and 90% under the solar and UV light respectively. These values were much higher than the bare TiO<sub>2</sub> where the degradation was only 70% and 57% under the solar and UV light irradiation. Similarly, the initial rate of reaction after 10 min and the rate constant was also observed to be highest with BZHT4 for which the values are provided in Tables 2 and 3. The degradations under solar light were observed to be 70%, 74%, 78%, 80%, 84% and 75% with BZHT0, BZHT1, BZHT2, BZHT3, BZHT4 and BZHT5 respectively. The final degradations under the UV light were 57%, 70%, 75%, 78%, 90% and 70% with BZHT0, BZHT1, BZHT2, BZHT3, BZHT4 and BZHT5

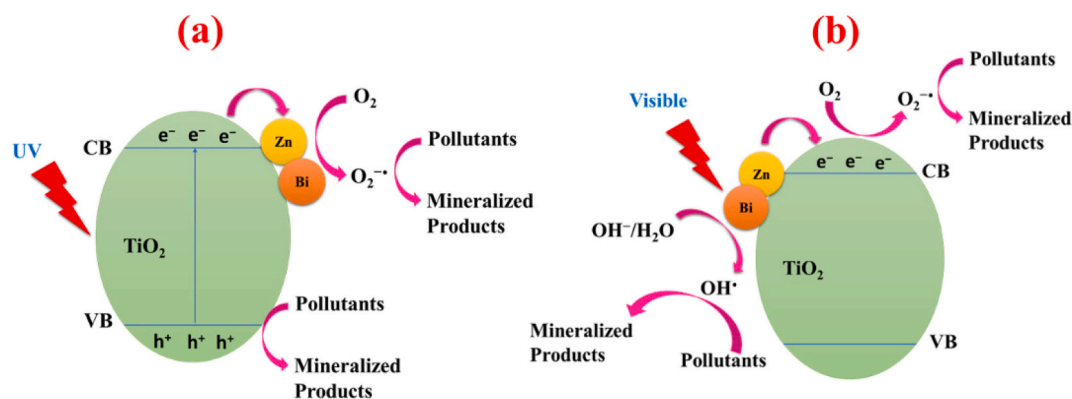


Fig. 4. Photocatalytic mechanism of metal doped TiO<sub>2</sub> under different light irradiations (a) under UV light and (b) under visible light.

respectively. The final percentage degradations were higher than the blank study where only 41% and 30% degradations were observed under solar and UV light respectively. These blank studies were conducted as reference, without addition of any catalyst and only in presence of light to confirm the role of catalyst in the degradation.

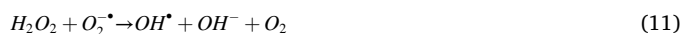
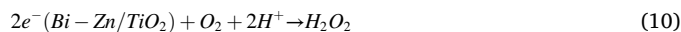
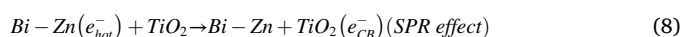
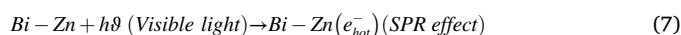
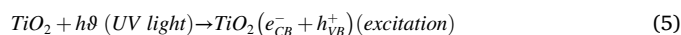
The higher photocatalytic activities of the metal doped catalysts could be attributed to the better light response for higher wavelength of light spectrum and charges separation in the BZHT1 to BZHT5 catalysts, that is probably due to the synergistic effect of Bi and Zn in the bimetallic Bi,Zn/TiO<sub>2</sub> nanoparticles. The response of doped catalysts to such higher wavelength of light spectrum is supported by their shift in band gap energies as given in Table 1. Along with this, synergistic effect and better charge separation with the mono and bimetal doping is also quite important and reported in earlier studies where similar efforts were performed [30,31]. Interestingly, all the metal doped TiO<sub>2</sub> catalysts showed remarkably reduced PL emission intensity in comparison to bare TiO<sub>2</sub>, which implies the diminished recombination of photogenerated electron-hole pairs, which is extremely advantageous for photocatalytic performance. It suggested that the efficient separation of photoinduced charge carriers at Bi–Zn junction with TiO<sub>2</sub> could extend the charge carrier lifetime. This shall further enhance interfacial charge transfer for broaden part of light spectrum under various light irradiation conditions. The results showed that an optimum concentration of Bi and Zn combination was required as in BZHT4 catalyst. Excess amount of Bi than the optimum value could lead to collision or/and an excessive number of defects, and excess amount of Zn than the optimum value act as recombination centers of electron-hole pairs, which reduce the performance. Therefore, BZHT1, BZHT2, BZHT3 and BZHT5 exhibited poor performance than BZHT4 [13].

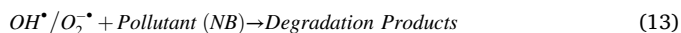
Another reason reported in literature for enhanced performance of doped TiO<sub>2</sub>, specially under solar light is the strong surface plasmon resonance (SPR) in visible region. Under the visible light, the electrons in the metal surface i.e., Bi and Zn are excited by photons of incident light which can be further transferred to TiO<sub>2</sub>, leading to better charge separation. There are studies which reports the SPR phenomenon shown by both Bi [32,33] and Zn metals [34]. The detailed charge transfer mechanisms of SPR phenomenon (in visible light) and charge separation in UV light is elaborated in mechanistic pathway section. However, the SPR effect is shown only by zero valent metals, it may also be possible for the in-situ reduction of Bi<sup>3+</sup> to Bi nanoparticles with UV light due to water splitting and lower metal loadings. These effects were not analyzed or confirmed in this work which can be further explored. The enhanced photocatalytic activity of the materials reported here is thus attributed only to the better light response for higher wavelength of light spectrum and charges separation. The photocatalytic performance of BZHT4 for NB degradation was compared the literature data of TiO<sub>2</sub> based catalysts as shown in Table S1.

### 3.3. Mechanistic approaches of photocatalysts in degradation of nitrobenzene

The mechanism of photocatalytic degradation of NB under the solar and UV light can be understood using the following equations from (5) to (13). Under UV light irradiation, TiO<sub>2</sub> being a semiconductor captures a UV light photon of appropriate energy and excites an electron ( $e^-$ ) from the valence band (VB) of TiO<sub>2</sub> to the conduction band (CB), leaving a hole ( $h^+$ ) behind (Eq. (5)). The excited  $e^-$  are then transported to the Bi–Zn bimetallic nanoparticles due to their lower energy levels (Eq. (6)). Bi–Zn nanoparticles act as co-catalyst and the close contact of Bi–Zn nanoparticles on TiO<sub>2</sub> introduces a potential gradient by the Schottky barrier between them (Fig. 4 (a)). Nevertheless, under visible light irradiation, Bi–Zn nanoparticles play the key role through SPR phenomenon. In this case, Bi and Zn act as sensitizer to accept the visible light photon (Fig. 4 (b)). After taking the photons of incident visible spectrum, electrons in the metal surface layer are excited (Eq. (7)). These  $e^-$  are further transferred to the CB of the TiO<sub>2</sub> as shown in Eq. (8). Since, the possible SPR effect is shown only by zero valent metals, which is not confirmed in this study. The Eqs. (7) and (8) are not applicable in the NB degradation in the current reported work.

These excited  $e^-$  from both the above processes react with adsorbed oxygen and water molecules to form superoxide radicals ( $O_2^{\bullet-}$ ) and afterwards hydrogen peroxide ( $H_2O_2$ ). This shall produce hydroxyl radicals ( $OH^{\bullet}$ ) in the reaction system (Eqs. (9–11)). On the other hand, the  $h^+$  in the VB of TiO<sub>2</sub> react with adsorbed water molecules and produce  $OH^+$  radicals (Eq. (12)). Both, these reactive species  $OH^+$  and  $O_2^{\bullet-}$  radicals further react with organic pollutant molecule NB to produce mineralized products  $CO_2$ ,  $H_2O$  and  $NH_4^+$  (Eq. (13)). Therefore, the combination of bimetals doping in TiO<sub>2</sub> can be effectively utilized in the improved photocatalytic activity for pollutant degradation. The contribution of these major active reactive radical species can be studied by applying suitable scavengers test which is not carried out in this study [35].





#### 4. Conclusions

In this study, all Bi—Zn doped TiO<sub>2</sub> catalysts showed enhanced activity for the photodegradation of NB under both UV and solar light irradiation. The optimum loading of Bi<sub>0.75</sub> and Zn<sub>0.25</sub> showed the highest activity with 90% and 84% NB degradation under UV and solar light irradiation. Furthermore, first order-kinetic model was applied for the degradation and the reaction rates were estimated. The enhanced photocatalytic activity of the catalytic materials was attributed to the synergistic effects between the doped metals on the TiO<sub>2</sub> and the efficient charge transfer between them.

#### Author contribution

Preeti: Investigation, Data curation; Saurav Mishra: Formal analysis, Writing - original draft; Nandana Chakinala: Investigation, Writing - review & editing; Anand G. Chakinala: Conceptualization, Validation, Visualization, Resources; Praveen K. Suroliya: Supervision, Funding acquisition, Methodology, Project administration.

#### Declaration of Competing Interest

The author declare that they have no known competing financial interests or personal relationships that could have appeared to influence the work reported in this paper.

#### Data availability

Data will be made available on request.

#### Acknowledgment

Authors thank ‘Central Analytical Facilities (CAF)’ and ‘Sophisticated Analytical Instrument Facility (SAIF)’, Manipal University Jaipur for providing the materials characterization facility. PKS acknowledge the funding support from Science and Engineering Research Board (SERB), India, under Grant No. [EMR/2016/006259].

#### Appendix A. Supplementary data

Supplementary data to this article can be found online at <https://doi.org/10.1016/j.catcom.2022.106538>.

#### References

- S.P. Kamble, S.B. Sawant, V.G. Pangarkar, Photocatalytic degradation of m-dinitrobenzene by illuminated TiO<sub>2</sub> in a slurry photoreactor, *Chem. Technol. Biotechnol.* 81 (2005) 365–371, <https://doi.org/10.1002/jctb.1405>.
- X. Yu, B. Kim, Kim Yu Kwon, Highly enhanced photoactivity of anatase TiO<sub>2</sub> nanocrystals by controlled hydrogenation-induced surface defects, *ACS Catal.* 11 (2013) 2479–2486, <https://doi.org/10.1021/cs4005776>.
- X. Zhu, Z. Liu, J. Fang, S. Wu, W. Xu, Synthesis and characterization of mesoporous Bi/TiO<sub>2</sub> nanoparticles with high photocatalytic activity under visible light, *J. Mater. Res.* 28 (2013) 1334–1342, <https://doi.org/10.1557/jmr.2013.92>.
- S.O. Flores, O. Rios-Bernij, M.A. Valenzuela, I. Córdova, R. Gómez, R. Gutiérrez, Photocatalytic reduction of nitrobenzene over titanium dioxide: by-product identification and possible pathways, *Top. Catal.* 44 (2007) 507–511, <https://doi.org/10.1007/s11244-006-0098-2>.
- A. Biswas, A. Corani, A. Kathiravan, Y. Infahsaeng, A. Yartsev, V. Sundstrom, S. De, Control of the size and shape of TiO<sub>2</sub> nanoparticles in restricted media, *Nanotechnology* 24 (2013) 195601, <https://doi.org/10.1088/0957-4484/24/19/195601>.
- P.K. Suroliya, M.A. Lazar, R.J. Tayade, R.V. Jasra, Nanocrystalline TiO<sub>2</sub> synthesized by sol-gel, solution combustion, and hydrothermal methods, *Ind. Eng. Chem. Res.* 47 (2008) 5847–5855, <https://doi.org/10.1021/ie800073j>.
- S. Dong, J. Feng, M. Fan, Y. Pi, L. Hu, X. Han, M. Liu, J. Sun, J. Sun, Recent developments in heterogeneous photocatalytic water treatment using visible light-responsive photocatalysts: a review, *RSC Adv.* 5 (2015) 14610–14630, <https://doi.org/10.1039/c4ra13734e>.
- P.A.K. Reddy, B. Srinivas, P. Kala, V.D. Kumari, M. Subrahmanyam, Preparation and characterization of Bi-doped TiO<sub>2</sub> and its solar photocatalytic activity for the degradation of isoproturon herbicide, *Mater. Res. Bull.* 46 (2011) 1766–1771, <https://doi.org/10.1016/j.materresbull.2011.08.006>.
- N. Chakinala, P.R. Gogate, C.A. Gupta, Highly efficient bi-metallic bismuth-silver doped TiO<sub>2</sub> photocatalyst for dye degradation, *Korean J. Chem. Eng.* 38 (2021) 2468–2478, <https://doi.org/10.1007/s11814-021-0890-5>.
- W. Bahnemann, M. Muneer, M.M. Haque, Titanium dioxide-mediated photocatalysed degradation of few selected organic pollutants in aqueous suspensions, *Cent. Mater. Sci.* 124 (2007) 133–148, <https://doi.org/10.1016/j.cattod.2007.03.031>.
- D. Vaya, P.K. Suroliya, Semiconductor based photocatalytic degradation of pesticides: an overview, *Environ. Technol. Innov.* 20 (2020) 101128, <https://doi.org/10.1016/j.eti.2020.101128>.
- P.K. Suroliya, R.J. Tayade, R.V. Jasra, TiO<sub>2</sub>-coated Cenospheres as catalysts for photocatalytic degradation of methylene blue, p -Nitroaniline, n -Decane, and n -Tridecane under solar irradiation, *Ind. Eng. Chem. Res.* 49 (2010) 8908–8919, <https://doi.org/10.1021/ie100388m>.
- J. Li, S. Cai, Z. Xu, X. Chen, J. Chen, H. Jia, J. Chen, Solvothermal syntheses of Bi and Zn co-doped TiO<sub>2</sub> with enhanced electron-hole separation and efficient photodegradation of gaseous toluene under visible-light, *J. Hazard. Mater.* 325 (2017) 261–270, <https://doi.org/10.1016/j.jhazmat.2016.12.004>.
- H. Li, J. Liu, J. Qian, Q. Li, J. Yang, Preparation of Bi-doped TiO<sub>2</sub> nanoparticles and their visible light photocatalytic performance, *Chinese, J. Catal.* 35 (2014) 1578–1589, [https://doi.org/10.1016/S1872-2067\(14\)60124-8](https://doi.org/10.1016/S1872-2067(14)60124-8).
- S. Murcia-López, M.C. Hidalgo, J.A. Navío, Synthesis, characterization and photocatalytic activity of Bi-doped TiO<sub>2</sub> photocatalysts under simulated solar irradiation, *Appl. Catal. A Gen.* 404 (2011), <https://doi.org/10.1016/j.apcata.2011.07.008>.
- S. Nasserli, M. Omidvar Borna, A. Esrafil, R. Rezaei Kalantary, B. Kakavandi, M. Sillanpää, A. Asadi, Photocatalytic degradation of malathion using Zn<sub>2+</sub>-doped TiO<sub>2</sub> nanoparticles: statistical analysis and optimization of operating parameters, *Appl. Phys. A Mater. Sci. Process.* 124 (2018), <https://doi.org/10.1007/s00339-018-1599-0>.
- B. Benalioua, M. Mansour, A. Bentouami, B. Boury, The layered double hydroxide route to Bi-Zn co-doped TiO<sub>2</sub> with high photocatalytic activity under visible light the layered double hydroxide route to Bi - Zn co-doped TiO<sub>2</sub> with high photocatalytic activity under visible light, *J. Hazard. Mater.* 288 (2015) 158–167, <https://doi.org/10.1016/j.jhazmat.2015.02.013>.
- P.K. Suroliya, R.J. Tayade, R.V. Jasra, Photocatalytic degradation of nitrobenzene in an aqueous system by transition-metal-exchanged ETS-10 zeolites, *Ind. Eng. Chem. Res.* 49 (2010) 3961–3966, <https://doi.org/10.1021/ie901603k>.
- I. Gul, M. Sayed, N.S. Shah, J. Ali, K. Polychronopoulou, Solar light responsive bismuth doped titania with Ti<sup>3+</sup> for efficient photocatalytic degradation of flumequine : synergistic role of peroxymonosulfate, *Chem. Eng. J.* (2019) 123255, <https://doi.org/10.1016/j.cej.2019.123255>.
- L. Yuliatli, N. Hasan, H.O. Lintang, Copper oxide modification to improve the photocatalytic activity of titanium dioxide nanoparticles: P25 versus P90, *InIOP Conf. Ser. Mater. Sci. Eng.* 902 (2020) 12010, <https://doi.org/10.1088/1757-899x/902/1/012010>.
- W. Chettah, S. Barama, M.-S. Medjram, M. Selmane, D. Montero, A. Davidson, J. C. Védrine, Anatase titania activated by Cu(II) or Zn(II) nanoparticles for the photooxidation of methanol assisted by Rhodamine-B, *Mater. Chem. Phys.* 257 (2021) 123714, <https://doi.org/10.1016/j.matchemphys.2020.123714>.
- V.N. Sonkusare, G.R. Chaudhary, G.S. Bhusari, A. Mondal, A.K. Potbhare, Raghvendra K. Mishra, H.D. Juneja, A.A. Abdala, Mesoporous octahedron-shaped Tricobalt tetroxide nanoparticles for photocatalytic degradation of toxic dyes, *ACS Omega.* 5 (2020) 7823–7835, <https://doi.org/10.1021/acsomega.9b03998>.
- M.F. Valan, A. Manikandan, S.A. Antony, A novel synthesis and characterization studies of magnetic Co<sub>3</sub>O<sub>4</sub> nanoparticles, *J. Nanosci. Nanotechnol.* 15 (2015) 4580–4586, <https://doi.org/10.1166/jnn.2015.9776>.
- S.M. Gupta, M. Tripathi, A review of TiO<sub>2</sub> nanoparticles, *Chin. Sci. Bull.* 56 (2011) 1639–1657, <https://doi.org/10.1007/s11434-011-4476-1>.
- P.R. Hemlata, A.P. Meena, K.K. Singh, Tejavath, biosynthesis of silver nanoparticles using Cucumis prophetarum aqueous leaf extract and their antibacterial and Antiproliferative activity against cancer cell lines, *ACS Omega.* 5 (2020) 5520–5528, <https://doi.org/10.1021/acsomega.0c00155>.
- R. Watanabe, A. Sugahara, H. Hagihara, J. Mizukado, H. Shinzawa, Molecular-scale deformation of polypropylene/silica composites probed by Rheo-optical Fourier-transform infrared (FTIR) imaging analysis combined with Disrelation mapping, *Anal. Chem.* 92 (2020) 12160–12167, <https://doi.org/10.1021/acs.analchem.0c00623>.
- S. Rajoriya, S. Bargole, S. George, V.K. Saharan, P.R. Gogate, A.B. Pandit, Synthesis and characterization of samarium and nitrogen doped TiO<sub>2</sub> photocatalysts for photo-degradation of 4-acetamidophenol in combination with hydrodynamic and acoustic cavitation, *Sep. Purif. Technol.* 209 (2019) 254–269, <https://doi.org/10.1016/j.seppur.2018.07.036>.
- S. Mishra, N. Chakinala, A.G. Chakinala, P.K. Suroliya, Photocatalytic degradation of methylene blue using monometallic and bimetallic Bi-Fe doped TiO<sub>2</sub>, *Catal. Commun.* 171 (2022) 106518, <https://doi.org/10.1016/j.catcom.2022.106518>.
- M. Kovatić, K. Perović, J. Papac, A. Tomić, L. Matoh, B. Žener, T. Brodar, I. Čapan, A.K. Surca, H. Kušić, U.L. Stangar, A. Lončarić Božić, One-pot synthesis of sulfur-doped TiO<sub>2</sub>/reduced graphene oxide composite (S-TiO<sub>2</sub>/rGO) with improved

- photocatalytic activity for the removal of diclofenac from water, *Mater. (Basel)*. 13 (2020) 1621, <https://doi.org/10.3390/ma13071621>.
- [30] W. Li, B. Li, M. Meng, Y. Cui, Y. Wu, Y. Zhang, H. Dong, Y. Feng, Bimetallic Au/Ag decorated TiO<sub>2</sub> nanocomposite membrane for enhanced photocatalytic degradation of tetracycline and bactericidal efficiency, *Appl. Surf. Sci.* 487 (2019) 1008–1017, <https://doi.org/10.1016/j.apsusc.2019.05.162>.
- [31] K.L. Reddy, S. Kumar, A. Kumar, V. Krishnan, Wide spectrum photocatalytic activity in lanthanide-doped upconversion nanophosphors coated with porous TiO<sub>2</sub> and Ag-Cu bimetallic nanoparticles, *J. Hazard. Mater.* 367 (2019) 694–705, <https://doi.org/10.1016/j.jhazmat.2019.01.004>.
- [32] W. Gu, F. Teng, SPR-promoted visible-light photocatalytic activity of Bi/ZIF hybrids, *J. Photochem. Photobiol. A Chem.* 400 (2020) 112679, <https://doi.org/10.1016/j.jphotochem.2020.112679>.
- [33] C. Zhou, C. Jiang, R. Wang, J. Chen, G. Wang, SPR-effect enhanced semimetallic BiO/p-BiOI/n-CdS Photocatalyst with spatially isolated active sites and improved carrier transfer kinetics for H<sub>2</sub> evolution, *Ind. Eng. Chem. Res.* 59 (2020) 8183–8194, <https://doi.org/10.1021/acs.iecr.0c00483>.
- [34] V. Chaurasia, N. Chand, S.K. Bajpai, Water sorption properties and antimicrobial action of zinc oxide nanoparticles-loaded cellulose acetate films, *J. Macromol. Sci. Part A*. 47 (2010) 309–317, <https://doi.org/10.1080/10601320903539207>.
- [35] R. Yadav, T.S. Chundawat, P.K. Surolia, D. Vaya, Photocatalytic degradation of textile dyes using  $\beta$ -CD-CuO/ZnO nanocomposite, *J. Phys. Chem. Solids* 165 (2022) 110691, <https://doi.org/10.1016/j.jpcs.2022.110691>.